PAPER • OPEN ACCESS

Effect of 3 T magnetic field on RF plasma sputtering in an ITER-relevant first mirror unit

To cite this article: Kunal Soni *et al* 2022 *Nucl. Fusion* **62** 126009

OPEN ACCESS
IOP Publishing | International Atomic Energy Agency Nuclear Fusion

Nucl. Fusion **62** (2022) 126009 (10pp) https://doi.org/10.1088/1741-4326/ac8b20

Effect of 3 T magnetic field on RF plasma sputtering in an ITER-relevant first mirror unit

Kunal Soni[1,*], Santhosh Iyyakkunnel[2,3], Roland Steiner[1], Rodrigo Antunes[1], Lucas Moser[1,4], Oliver Bieri[2,3], Laurent Marot[1] and Ernst Meyer[1]

[1] Department of Physics, University of Basel, Klingelbergstrasse 82, CH-4056, Basel, Switzerland
[2] Division of Radiological Physics, Department of Radiology, University Hospital Basel, Petersgraben 4, CH-4031, Basel, Switzerland
[3] Department of Biomedical Engineering, University of Basel, Gewerbestrasse 14, CH-4123, Allschwil, Switzerland
[4] ITER Organization, Route de Vinon-sur-Verdon—CS 90 046—13067 St Paul Lez Durance Cedex, France

E-mail: kunaldhirajal.soni@unibas.ch

Received 11 May 2022, revised 6 August 2022
Accepted for publication 19 August 2022
Published 20 October 2022

Abstract

The first mirror (FM) cleaning operations in ITER are expected to be executed in the presence of a ∼3 T magnetic field. In the RF plasma cleaning configuration, this would have a significant influence on the plasma properties, ion energy, angle of incidence as well as flux spatial distribution. To this end, RF discharges were excited in an ITER-sized mock-up of a first mirror unit (FMU) consisting of a powered first mirror M1 and a grounded second mirror M2 placed in a homogeneous 3 T magnetic field. The plasma discharge was confined in a beam extending in the direction of the magnetic field, consequently wetting a limited portion of the FMU walls. In the DC-decoupled scheme (without $\lambda/4$ filter), this considerably influenced the self-bias voltage V_{DC} that develops on M1. Changing the angle α between M1 normal and magnetic field, modified the plasma wetted wall area A_g and the resulting V_{DC} varied by over two orders of magnitude. Plasma exposure experiments were also done in the DC-coupled scheme (with $\lambda/4$ filter), wherein the angle and wetted surface determined the area of wall sputtered. Increasing α led to an increase in the sputtered wall area A_g, and consequently the wall deposition on grounded M2. However, in all the cases M1 was entirely clean with the exception of edge deposits in some. In contrast, both M1 and M2 are coated with wall deposits in the absence of a magnetic field and a similar plasma exposure. The results show that plasma cleaning with $\lambda/4$ filter in a 3 T magnetic field at ITER could potentially prevent the parasitic wall deposition on FMs. The results also highlight the importance of FM orientation in the magnetic field and the wetted area in the plasma cleaning in both the DC-coupled and decoupled schemes within the ITER diagnostic systems.

Keywords: RF plasma, magnetic field, first mirror, notch filter, ITER

(Some figures may appear in colour only in the online journal)

* Author to whom any correspondence should be addressed.

1. Introduction

Metallic first mirrors (FMs) make up important components in a majority of the optical diagnostic systems in the fusion reactor ITER. They are responsible for directing the light from the fusion plasma towards the diagnostic sensors through an optical labyrinth to prevent neutron leakage. However, being the initial elements in the optical path, the FMs are subject to constant erosion from charge exchange neutrals as well as deposition of the first wall materials: beryllium (Be), tungsten (W) and their oxides, which would significantly degrade their optical properties [1, 2]. The first wall depositions and a corresponding loss in FM reflectivities had already been reported post experimental campaigns in the JET-ILW tokamak [3, 4]. The FMs would hence require regular cleaning to restore their optical properties which, among other techniques, is foreseen to be achieved by *in situ* capacitively coupled radio-frequency (CCRF) plasma cleaning technique [5]. This technique employs FMs as the powered electrode, feeding RF directly to it. The asymmetry between the surface area of FM (powered electrode) and the plasma-wetted walls of the diagnostic duct (grounded electrode) leads to development of a negative self-bias potential V_{DC} on the FM [6]. This results in ion acceleration towards the FM with an energy of $e(V_p - V_{DC})$, where V_p is the plasma potential, and leads to sputtering of surface deposits given the ion energy is greater than the sputtering energy threshold of the deposits. Plasma cleaning of FM deposits via CCRF discharges has been a subject of intense investigation in recent years [7–10].

The FMs in some diagnostic systems would also be actively water-cooled to tackle the high thermal loads deposited on the mirrors via gamma and neutron radiation. The physical contact of the grounded water cooling lines with the FMs however leads to their RF grounding, disabling the generation of CCRF discharges. To overcome this challenge, the water cooling lines are foreseen to be implemented as a quarter-wavelength ($\lambda/4$) filter [5, 11]. Adding a $\lambda/4$ filter DC-grounds the FMs while allowing the RF to propagate through them, leading to the generation of RF plasma for mirror sputtering purposes. However, this also leads to an increase of the V_p to several hundred volts [12–15], which in turn increases the sputtering of wall surfaces surrounding FMs. The sputtered wall material in turn gets deposited on the FMs making the plasma cleaning process less effective [16]. Hence CCRF plasma cleaning with a $\lambda/4$ filter requires additional mitigation strategies to achieve FM cleaning [16, 17].

In ITER, the majority of the mirror cleaning operations are expected to be executed in the presence of the toroidal magnetic fields in the range of 3 to 3.8 T at the locations of the FMs [5]. The presence of fields of this magnitude would significantly influence the cold plasma properties, particularly the bias voltage on the mirror, ion directionality and flux spatial distribution, all of which can significantly affect the mirror cleaning rate and uniformity [18, 19]. Hence, it is crucial to investigate plasma cleaning of FMs in presence of strong magnetic fields. Despite its importance, there have been only a handful of published studies focused on mirror cleaning in magnetic fields. Razdobarin *et al* studied the uniformity of FM sputtering in 0.05 T magnetic field using 81.36 MHz RF discharges [20]. They reported an enhanced sputtering rate at the centre of the electrode, but also noted that the longitudinal field improved sputtering uniformity along the edges. They also indicated that the net sputtering profile in magnetic fields is determined not only by the ion flux distribution but also by the re-deposition process. Rogov *et al* performed cleaning experiments with Penning discharges using helium plasma in a magnetic field up to 0.5 T [21]. They noted an efficient cleaning of molybdenum (Mo) mirrors from aluminium (Al) coatings (used as a Be proxy [22]) up to 200 nm while recovering the optical properties of the mirror. Moser *et al* also reported the cleaning of Mo mirrors from Al_2O_3 films (serving as BeO proxy) with 13.56 MHz RF plasma using argon (Ar) as process gas in a magnetic field of 0.35 T [23]. The cleaning performance was particularly enhanced when the field lines were nearly parallel (within a few degrees) to the mirror surface. In another study, they also performed plasma erosion experiments in 3.5 T field [24]. They reported the formation of filaments as well as strong inhomogeneities due to erosion profile drifts on the FM surface, with the ratio between the maximum and minimum erosion rate on the FM sample being as high as 14. Yan *et al* conducted CCRF plasma cleaning experiments on the edge Thompson scattering mock-up in 1.7 T magnetic field of the EAST tokamak [25]. The presence of magnetic field reportedly lowered the self-bias on the FMs up to a factor of 10, and the cleaning rate increased by a factor of 40 when compared to identical experiments without a magnetic field. They also reported a complete recovery of the total reflectivity of the FMs, while the diffuse reflectivity and surface roughness at the centre was enhanced most likely as a result of asymmetric surface sputtering in the magnetic field. In a recent study, Shigin *et al* presented experimental results describing the impact of an axial 0.5 T field on CCRF discharges in the DC-coupled (with $\lambda/4$ filter) scheme, wherein they observed a lowering of the DC current with magnetic field [5]. Furthermore, the effect of the field was more pronounced at lower excitation frequencies, and at fields $\geqslant$0.3 T (where both ions and electrons are magnetized) the ion energies obtained were identical both in the presence as well as in absence of the $\lambda/4$ filter.

Aside from the above-mentioned works, there has been a significant lack of research into RF discharge sputtering in magnetic fields. In this article, we extend the knowledge further by investigating the RF discharges as well as plasma surface interactions using a mock-up of a first-mirror unit (FMU) relevant to ITER in 3 T. We conduct research on both the DC-coupled and DC-decoupled schemes, given the diagnostic systems in ITER will implement FM cleaning in either of the configurations. In the DC-decoupled scheme (without $\lambda/4$ filter), we study the impact of process parameters as well as FM orientation with magnetic field on the self-bias voltage developed on FMs. In the DC-coupled scheme (with $\lambda/4$ filter) we study the RF discharges, wall sputtering and parasitic deposition on FMs in varied orientations of the FMU with the magnetic field. This is the most relevant configuration

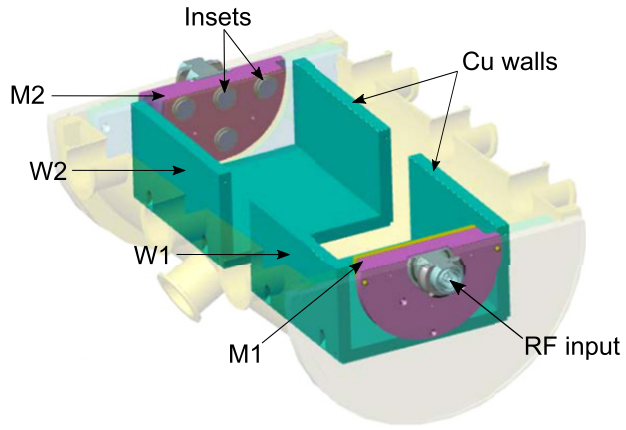

Figure 1. Sectional view of the FMU (CAD drawing).

yet of RF discharge mirror sputtering for ITER, and the results provide considerable implications for ITER.

2. Experimental

The experiments were performed in an FMU mock-up, which was assembled inside a cylindrical vacuum chamber with a length of 340 mm and a diameter of 254 mm. The CAD drawing of the FMU is presented in figure 1. The FMU held two circular unpolished molybdenum (Mo) electrodes, M1 and M2, with a diameter of 120 mm. M1 and M2 represent the first and second mirrors respectively and were placed in grounded holders on the opposite ends of the FMU. They held 5 circular insets each with a diameter of 18 mm. The insets made of bulk Mo as well, were electrically connected to the electrodes and could be detached for surface characterization. M1 was used as the powered electrode while M2 was kept electrically grounded. Two hollow cubes made of copper (Cu) (indicated as W1 and W2 in figure 1) were placed inside the vacuum chamber, adjacent to M1 and M2 as indicated in figure 1. These cubes served as the 'walls' of the FMU. The hollow cubes were electrically connected to the body of the vacuum chamber, and served as the grounded electrode. A 60 MHz RF generator (Comet cito) coupled with a matchbox was used to generate a 1 Pa helium (He) or argon (Ar) plasma inside the FMU. To minimise the RF power losses, low-loss co-axial cables (S 10172 B-11 Huber + Suhner) were used for power transmission. Additionally, a pre-matching capacitor was used at the powered electrode to further limit the RF power [26].

The geometrical area of the powered electrode (A_p), M1, was 157 cm^2, while the internal surface area of the grounded hollow cubes (A_g) was 3567 cm^2, leading to a ratio of $A_g/A_p \approx 15$. Due to the area asymmetry, a CCRF discharge leads to the development of a negative self-bias on M1. This bias voltage is directly indicated on the display of the RF generator. For several experiments, this DC bias was short-circuited by the addition of a $\lambda/4$ filter at the powered electrode. The details of the $\lambda/4$ filter (or notch-filter) are presented in [16]. Consequently, a CCRF discharge is excited while DC grounding the powered electrode at the same time.

The experiments with magnetic field were performed at the University Hospital Basel employing the 3 T field from

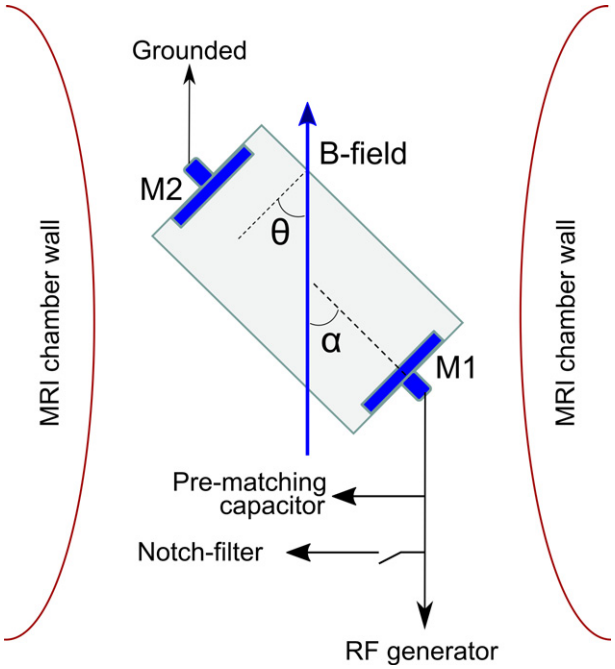

Figure 2. Top view schematic representation of the FMU inside the MRI bore.

a clinical magnetic resonance imaging (MRI) system (MAGNETOM Prisma by Siemens Healthcare). The static magnetic field is generated using superconducting solenoid coils that are cooled with liquid He using zero boil off technology. The magnetic field in the bore (600 mm diameter and 2 m length) has homogeneity of about 1 ppm over a volume with a diameter of 500 mm. The FMU was placed in the magnetic isocenter, and could be rotated so as to vary the angle between the surface normal of M1 and the magnetic field (oriented along the bore of the MRI system). This angle is referred to as α in this manuscript. A schematic representation displaying the FMU and the angle α is presented in figure 2. The room where the MRI system is located is equipped with RF shielding against interference to/from electronic equipment as well as passive magnetic shielding to attenuate the magnetic field outside the room. The FMU was brought to a base pressure between 10^{-4} and 10^{-3} Pa via a turbo-molecular pump placed outside the room. The RF generator (with match-box) was also placed outside the room along with the pumping unit. The vacuum connection, gas supply and RF connections were made via long (>6 m) lines and cables. An image of the FMU in the MRI bore with the necessary connections is displayed in figure 3.

The pressure measurements during the experiments were done via the Penning gauge attached to the pumping system (above the turbo pump). However, it is worth noting that the pressure in the FMU differs from that at the pumping system, given that it is pumped via 6 m long lines. Hence, prior to performing experiments, a pressure calibration test was done using He and Ar gases by mounting a Baratron gauge on top of the FMU in absence of a magnetic field. This way the pressures inside the FMU were known for a given flow of the gas and linked with the pressures at the pumping system. For the experiments in the magnetic field, the Baratron gauge was

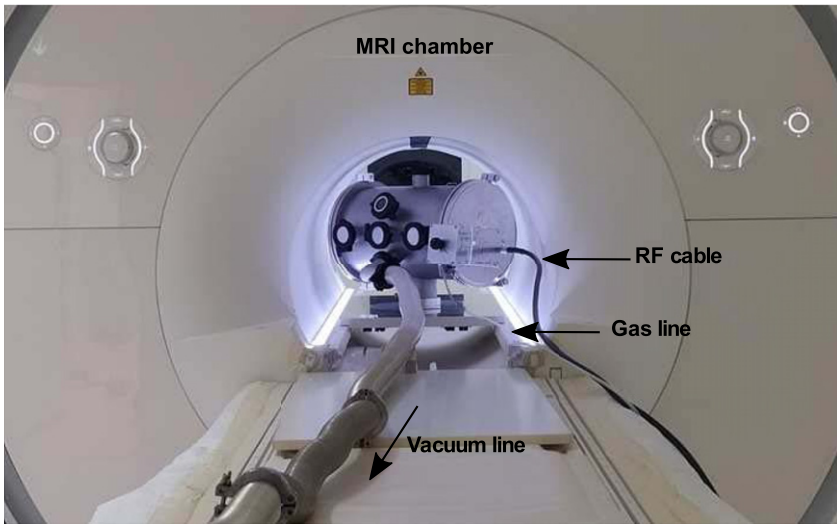

Figure 3. Image of the experimental setup displaying the FMU inside the MRI bore, with the necessary connections in the setup.

dismounted from the FMU and the pressure inside the chamber was monitored using the calibration results for a given flow.

The insets of M1 and M2 were characterised after relevant experiments using energy-dispersive x-ray spectroscopy (EDX). The thickness of surface layers was obtained by fitting the EDX data via the STRATAGem software [27–29], the procedure of which is described elsewhere [30]. The EDX measurements were performed with the SEM-FEI Nova Nano SEM23 microscope, varying the acceleration voltage from 3 to 20 kV.

3. Results and discussion

3.1. Impact of discharge parameters—DC decoupled scheme

To begin with, RF discharges with argon were generated in the FMU in the DC-decoupled scheme (without $\lambda/4$ filter). Evidently, this leads to the development of a negative self-bias voltage V_{DC} on the powered electrode M1. Measurements were performed in 3 T to study the V_{DC} on M1 as a function of varying RF power as well as the angle α (figure 2). Experiments were also done in absence of the magnetic field for reference.

The RF power was varied from 50 to 300 W, keeping the Ar pressure and α constant at 1 Pa and 45°, respectively. In 3 T field, the $|V_{DC}|$ on M1 increases monotonically with RF power as displayed in figure 4. In a CCRF plasma with a high excitation frequency (like 60 MHz used in our experiment), the sheath at the electrodes is primarily capacitive and the V_{DC} developed on the powered electrode can be represented as [13]

$$|V_{DC}| = V_{RF}\left(\frac{C_g - C_p}{C_g + C_p}\right), \tag{1}$$

where V_{RF} is the RF potential on the powered electrode, C_p and C_g are the sheath capacitances at the powered and grounded (wall) electrode, respectively. The magnitude of the sheath capacitances in this expression can be obtained as

$$C = \epsilon_0 \frac{A}{L}, \tag{2}$$

where ϵ_0 is the vacuum permittivity, L is the mean sheath thickness and A is effective area of the electrode in contact with the plasma. Using this relation, equation (1) can be re-written as

$$|V_{DC}| = V_{RF}\frac{(A_g/A_p) - (L_g/L_p)}{(A_g/A_p) + (L_g/L_p)}, \tag{3}$$

where A_g and A_p are the effective areas, and L_g and L_p are the sheath thicknesses at the grounded and powered electrodes, respectively. As can be inferred from equation (3), $|V_{DC}|$ on the powered electrode is determined primarily by V_{RF}, the effective area ratio A_g/A_p and the ratio of sheath thickness L_g/L_p. As the RF power is increased, the V_{RF} at the electrode increases explaining the rise in $|V_{DC}|$ as observed in figure 4 in accordance with equation (1). In absence of magnetic field (0 T), the $|V_{DC}|$ increases with RF power in a similar fashion (figure 4). However, at any given power $|V_{DC}|$ is larger at 0 T in comparison to 3 T. This is attributed to the differing grounded areas A_g in the two cases. At 0 T, the plasma expands in the entire FMU, leading to maximum A_g and consequently the area ratio A_g/A_p (∼15). In the presence of magnetic field, the plasma is confined in a cylindrical column extending from M1 in the direction of $\vec{B}$, as can be observed in figure 5. This can be understood schematically via the illustration presented in figure 6. As a result, the plasma column wets only a portion of the grounded wall depending on the orientation of the FMU in the magnetic field. This wet portion makes up the effective grounded area A_g. Hence, at 3 T A_g is significantly lower compared to 0 T at the same V_{RF}, lowering the area ratio A_g/A_p from 15 to 1 and consequently the $|V_{DC}|$. This explains the vertical shift in the $|V_{DC}|$ plot for 0 and 3 T in figure 4.

Further, the FMU was rotated in magnetic field to vary the angle α between 0° and 80°, keeping the RF power and Ar pressure constant at 120 W and 1 Pa, respectively. The $|V_{DC}|$ at the electrode is experimentally measured and is displayed at the RF generator. As indicated in figure 7(*a*), the $|V_{DC}|$ initially increases attaining a maximum at $\alpha \sim 15°$. Upon further increase in α, $|V_{DC}|$ decreases monotonically, and for $\alpha > 50°$, $|V_{DC}|$ approaches 0 V. This change in $|V_{DC}|$ with α can also be

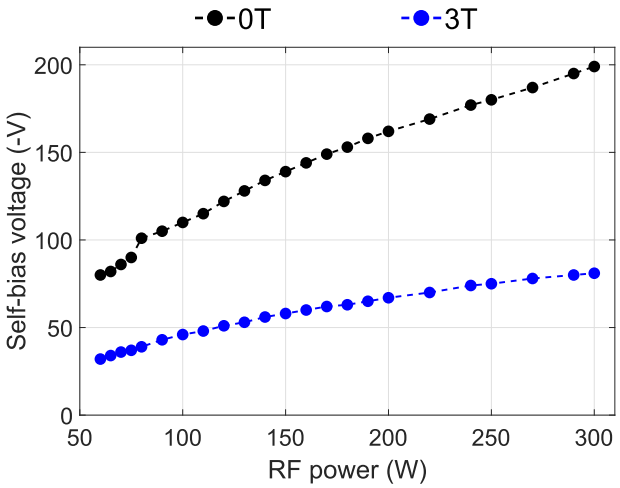

Figure 4. Experimentally measured self-bias voltage on the powered electrode (displayed in units of −V) with varying RF power (constant pressure of 1 Pa) in presence of 3 T and 0 T B-fields. α is constant at 45°.

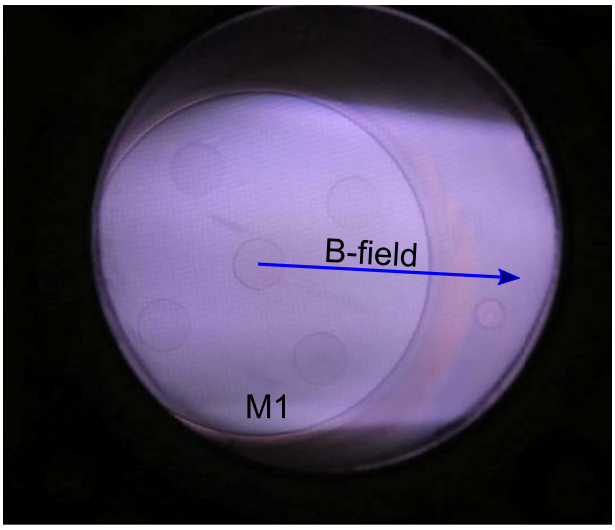

Figure 5. Image of the confined plasma column extending from M1 in the direction of magnetic field.

explained on the basis of change in the wetted ground area A_g, where A_p being the area of M1 remains constant. While the wetted areas were not measured experimentally, the geometric A_g can be calculated by taking projection of the cylindrical plasma column extending from M1 onto the wall in the direction of the field as indicated in figure 6. The resulting area ratio A_g/A_p at the corresponding α is presented in figure 7(*b*). As can be inferred, $|V_{DC}|$ varies in an similar manner to that of A_g/A_p with changing α. At $\alpha = 0°$, the plasma column wets M2 which makes up the effective A_g, leading to $A_g/A_p \sim 1$. Increasing α, the plasma column wets the wall adjacent to M2 increasing the A_g/A_p until it reaches a maximum of 2.85 at $\alpha = 15°$. Increasing the α further only decreases the A_g as indicated in figure 6, and for $\alpha > 60°$ the A_g/A_p effectively approaches 0 (figure 7(*b*)). The results clearly indicate that the $|V_{DC}|$ in magnetic field depends significantly on the wetted ground area by the plasma column, and can be varied by as much as a factor of 100 by simply changing the orientation of the FM with the magnetic field. It is important to note that the A_g/A_p values presented in figure 7(*b*) is a simplified calculation based on geometrical projection of the plasma column on the side wall at varied angles. However, the real A_g/A_p may differ from the calculated values considering the possibility of an incomplete wetting of the side walls at certain angles, as will be discussed in the next section. It is also worth noting that even though the RF power is constant, the V_{RF} at the electrode might fluctuate due to RF losses and impedance fluctuations in the pre-matching circuit. This could also contribute to an uncertainty in the $|V_{DC}|$ measurements.

In absence of magnetic fields (0 T), the ratio of sheath thicknesses L_g/L_p does not play a significant role in the determination of $|V_{DC}|$ in asymmetrical electrode systems like ours, as A_g/A_p is at least one order of magnitude larger than L_g/L_p [12]. This is primarily the result of plasma expansion in the chamber volume, which maximises A_g and consequently A_g/A_p, making it the dominant term in equation (3). However, at 3 T, A_g/A_p is lowered considerably by the virtue of plasma confinement. Now, as the order of A_g/A_p approaches that of L_g/L_p, the latter can no longer be neglected and it might even play a defining role in the determination of $|V_{DC}|$. Moreover, L_g, as well as L_p, can differ at varied angles due to the presence of the Chodura sheath [31]. However, we cannot comment on the impact quantitatively for the lack of experimental data on L_g and L_p. Dedicated studies are necessary to experimentally measure L_g/L_p and its influence on $|V_{DC}|$ in strong magnetic fields. In addition, mirror cleaning experiments in the DC-decoupled scheme are also necessary to study the net impact of the above mentioned effects such as incomplete wall wetting, $|V_{RF}|$ fluctuations and role of magnetized sheaths on the mirror erosion and depositions.

The results have considerable implications for plasma cleaning of DC-decoupled mirrors in ITER diagnostics. The ion energy on the FM in such configuration is given by $e(V_p - V_{DC})$ and hence depends directly on self-bias voltage. As a result, the ion energy on FM would vary considerably with its orientation with magnetic field. This could particularly be an issue at grazing angles ($\alpha > 70°$) where the self-bias voltage approaches 0 V and the ion energies could reach relatively low values. This could potentially be countered by increasing the wetted area A_g by making geometrical modifications to the wall surface, such as using shaped wall structures rather than flat surfaces. The impact of such geometrical modifications on the resulting self-bias voltage however requires further investigation.

3.2. Plasma sputtering experiments—DC coupled scheme

Further, we performed plasma sputtering experiments in the FMU in the DC-coupled scheme (with $\lambda/4$ filter), to study the wall sputtering and deposition on M1 and M2 during plasma discharge in magnetic fields. Adding a $\lambda/4$ filter leads to DC-grounding of M1 ($|V_{DC}| = 0$ V) and a considerable rise in the plasma potential V_p [12, 16]. M2 was kept electrically grounded as well. Some pieces of silicon (Si) wafers were

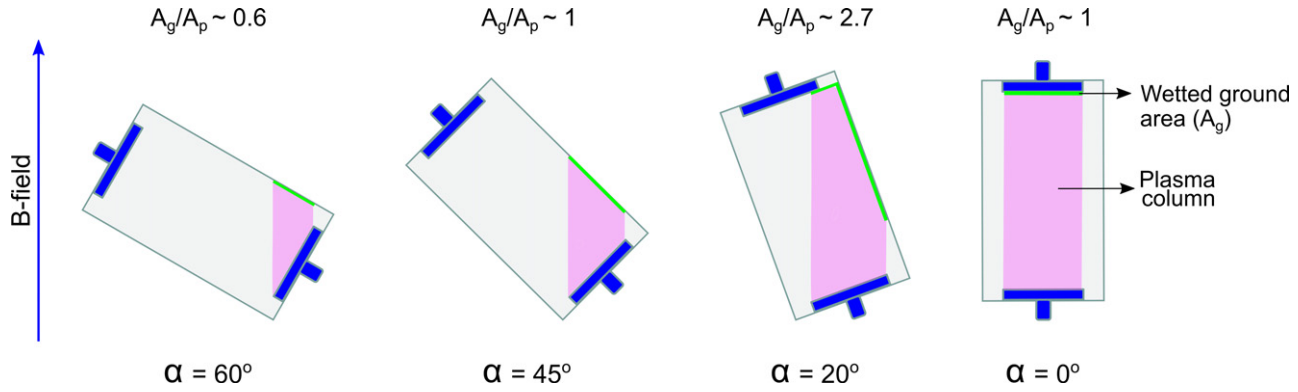

Figure 6. Illustration of the plasma column in magnetic field and the corresponding wetted ground area A_g in the FMU, with varying angle α.

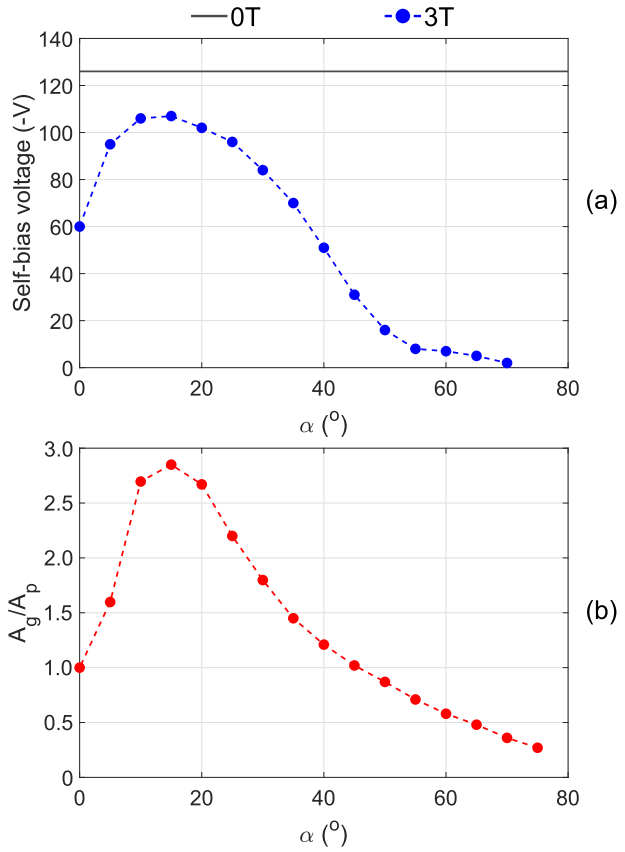

Figure 7. (*a*) Experimentally measured self-bias voltage on the powered electrode (displayed in units of −V) and (*b*) geometrical area ratio (calculated) between the wetted grounded area by the plasma column and the powered area A_g/A_p with varying α. RF power and Ar pressure are constant at 120 W and 1 Pa, respectively.

also placed on M2, which were electrically floating over the experimental duration. In a typical discharge, they acquire the positive floating potential V_f, wherein the ions reach their surface with an energy corresponding to $e(V_p - V_f)$. This is typically in the range of ∼10 eV, which is considerably low to cause any surface sputtering of the Si samples. As a result, they accumulate all the deposits that reach its surface without getting sputtered back, giving insight into the wall sputtering and total rate of deposition [16]. For this study helium was used as the discharge gas, as it reportedly leads to wall depositions on FMs during plasma cleaning with $\lambda/4$ filter in absence of magnetic field [16], allowing us to make an effective comparison when doing similar experiments in 3 T field.

Initially, an experimental discharge was conducted without magnetic field to serve as a reference. The discharge was generated with an RF power of 55 W and allowed to run for 8.5 h. The plasma potential V_p as measured by a Langmuir probe (HIDEN's ESPion^{TM}) was roughly 60 V at these parameters, corresponding to ion energy of ∼60 eV on M1, M2 as well as on the walls. In the absence of a magnetic field, the plasma expands throughout the FMU, maximising the area of the walls sputtered. After the experiment, the surfaces of both M1, as well as M2, were deposited with Cu as observed in figure 8. EDX analysis on the insets of M1 indicated a Cu deposition of 3–4 nm in thickness. As can be observed in figure 8(*a*), the deposition was greater towards the edges of M1 in proximity to the walls. It is worth noting that the entire M1 was clean prior to the experiments, hence all deposition observed in figure 8(*a*) is entirely a result of the wall sputtering during the experiments. EDX analysis was performed on the central inset of M2 which yielded a Cu deposition of 3–4 nm. Hence, the net wall deposition on both M1 and M2 is identical, which is understandable owing to the geometrical symmetry and the fact that both are in a DC-grounded state. One must not be confused by the fact that M2 looks differently coated compared to M1 in figure 8. This is merely due to the fact that the surface of M2 was not cleaned prior to the experiment, and had accumulated deposits from previous experimental trials. Only the central inset and the Si samples on M2 were replaced before this experiment, and hence we only consider the deposition measured on them instead of the entire M2. EDX analysis on the floating Si samples placed on M2, indicated a Cu deposition of roughly 35 nm, leading to a deposition rate R_D of 4.1 nm h^{-1}. To recall, this is the total deposition rate at M2, excluding any erosion. While no such measurements were done on M1, R_D on its surface is expected to be similar for the reasons mentioned earlier. Being DC-grounded, M1 and M2 are also sputtered with a considerably larger ion energy of $eV_p \sim 60$ V. Hence the erosion on their surfaces (with the erosion rate R_E) competes with a subsequent deposition of the

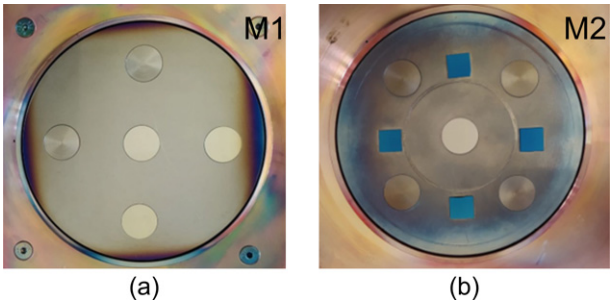

Figure 8. Images of (*a*) M1 and (*b*) M2 after experiment in 0 T.

wall material (with rate RD) during the discharge. The net impact is the 3–4 nm equivalent Cu thickness on the mirror surfaces, indicating they are in a net deposition regime, i.e. $R_D > R_E$ over the discharge duration.

Following that, an identical experiment was done in the magnetic field at $\alpha = 45°$. The surfaces of M1 and M2 were sandblasted to remove any previous deposits, before conducting this experiment. Unfortunately, the plasma properties and ion energy at surfaces in FMU cannot be measured with conventional diagnostic tools in the 3 T field. Hence, we discuss only the qualitative effects of plasma sputtering and wall deposition upon constant parameters in the magnetic field. The discharge was excited with an RF power of 200 W, with a discharge duration of 3 h. At $\alpha = 45°$, the plasma extends in a cylindrical column in the direction of magnetic field, wetting the wall surface directly adjacent to M1 (illustrated in figure 9) with $A_g/A_p \sim 1$. Post the experimental discharge, a circular region was sputtered on the wall adjacent to M1, directly corresponding to the wetted area by the plasma column as indicated in figure 9(*a*). In 3 T field, the ion flux in the plasma column is expected to be considerably larger than that obtained without magnetic fields, leading to an increased sputtering yield in the wetted region. Furthermore, the ions impact the wetted surface at a non-normal incidence due to the presence of a Chodura sheath in addition to a Debye sheath between the bulk plasma and the grounded wall [31]. The impact angle of the ions depend on the orientation of the magnetic field with the wall surface normal, represented by θ in figure 2. The impact angle is typically lower than θ [32], and scales with the increasing θ [31]. A steeper ion impact angle coupled with increased ion flux and energy is typical of an increased sputtering yield [33], which can be assumed for the wet surfaces in the FMU. M2 was visually clean of deposits as observed in figure 9(*b*). EDX measurement on the central inset of M2 revealed a Cu thickness of 3–4 nm, indicating minimal deposition. The floating Si samples also indicated a Cu deposition of 3–4 nm, identical to that obtained on the inset of M2. The fact that the floating Si samples and grounded inset on M2 have the same deposition hint towards a lack of erosion on its surface. This can be understood, since the plasma column does not wet the surface of M2 leading to an absence of ion sputtering and hence erosion. Moreover the minimal surface deposition (3–4 nm) can be attributed to the fact that the wall surface sputtered by the plasma column is at a considerable distance from M2. It is worth noting that prompt re-deposition is also relevant in 3 T fields [34], i.e.,

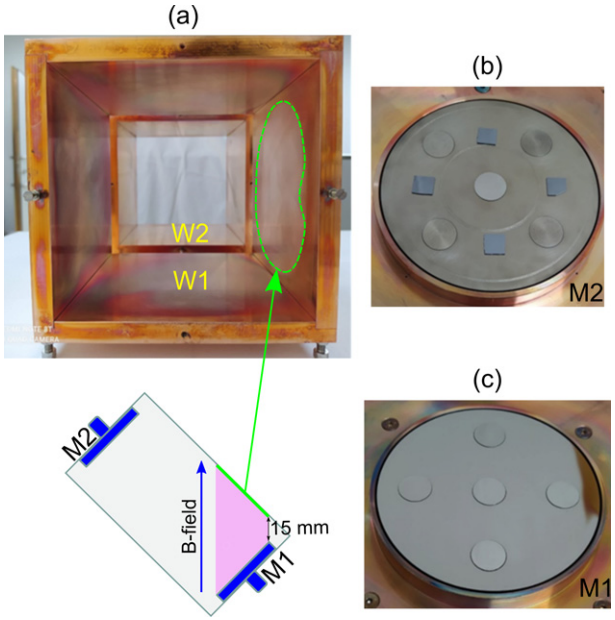

Figure 9. Images of the (*a*) FMU wall, (*b*) M2 and (*c*) M1 after experiment in 3 T field and $\alpha = 45°$. The sputtered region relevant to $\alpha = 45°$ on W1 is indicated via the dotted line.

depending on certain factors the sputtered Cu atoms from the walls can be ionized in the Debye sheath, and be re-deposited back on the wall surfaces. This could lower the net sputtering yield, contributing to a lower deposition on M2. However, it is difficult to comment on the degree of prompt re-deposition, if any, in our experiments. Interestingly, the surface of M1 was visually clean except for at the edge as observed in figure 9(*c*). EDX analysis on the insets of M1 also indicated no presence of Cu, verifying that M1 was in an erosion dominant regime during the experiment, i.e., $R_E > R_D$. The portion of M1 with Cu deposition was the edge closest to the adjacent wall with a distance of 15 mm. We speculate that this connection length is too low to sustain a plasma discharge in the gap. As a result, the M1 edge only receives the sputtered wall deposits without undergoing erosion, leading to accumulation of Cu on the edge. However, on the remainder of M1 the plasma erosion outweighs the wall deposition, resulting in a clean surface. Furthermore, the wall surface directly adjacent to the deposited edge of M1 was also visually unsputtered as displayed in figure 9(*a*). This observation further supports the speculation the concerning absence of plasma discharge in the 15 mm gap between the M1 edge and the adjacent wall.

Lastly, an experiment was performed in magnetic field with $\alpha = 20°$. The surfaces of M1 and M2 were sandblasted to remove the previous deposits before conducting this experiment. The discharge was generated with 200 W RF power for a duration of 3 h. As α is changed from 45° to 20°, the plasma column wets a much larger surface of the adjacent walls as indicated in figure 6, with A_g/A_p increasing from $\sim$1 to $\sim$2.7. Visual inspection after the experimental discharge indicated an elliptical sputtered portion on the walls adjacent to M1, again corresponding to the wetted area by the plasma column as displayed in figure 10(*a*). M2 was considerably coated with wall deposits upon visual observation as observed

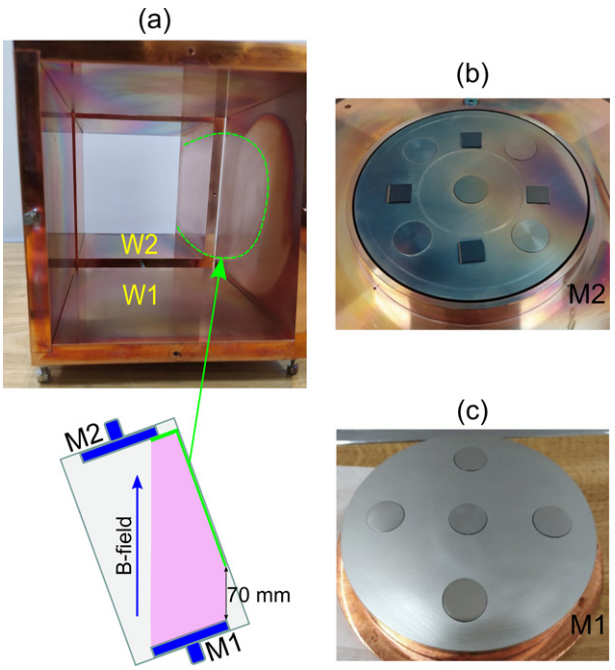

Figure 10. Images of the (*a*) FMU wall, (*b*) M2 and (*c*) M1 after experiment in 3 T field and $\alpha = 20^{\circ}$. The circular sputtered pattern observed on W1 is the remnant of the experiment conducted at $\alpha = 45^{\circ}$, and the sputtered region relevant to $\alpha = 20^{\circ}$ is indicated via the dotted line.

in figure 10(*b*). EDX analysis on the insets of M2 displayed a Cu thickness ranging from 27 to 47 nm. On the floating Si samples, the Cu thickness was obtained between 19 and 54 nm. The equivalent deposition on the grounded insets as well as the floating Si samples on M2 is again indicative of a lack of erosion on the surface of M2. As in the $\alpha = 45^{\circ}$ experiment, this can be explained based on a lack of wetted region on M2 by the plasma column. The total deposition on M2 however is significantly larger than that obtained at $\alpha = 45^{\circ}$ ($\sim$3 nm). This is because a larger wall surface is wet and sputtered in this case, which is also in close proximity to M2 as observed in figure 10(*a*). Furthermore, the θ in this case, is also larger (70°) compared to that in the experiment with $\alpha = 45^{\circ}$, where θ was also 45°. A larger θ implies a larger ion impact angle on the wet wall surface and consequently a larger sputtering yield. Hence, increased sputtering yield and deposition from the sputtered wall adjacent to M2 combined with a lack of M2 erosion due to absence of plasma interaction results in a net deposition as high as 50 nm. The entire surface of M1 was visually clean without any edge deposition (figure 10(*c*)). EDX analysis on the insets of M1 detected no Cu, verifying the absence of deposits and an erosion-dominant regime or $R_{\mathrm{E}} > R_{\mathrm{D}}$ on its surface. It is worth noting that the minimum connection length between the M1 edge and the adjacent wall in this configuration is 70 mm (compared to 15 mm at $\alpha = 45^{\circ}$). A larger connection length in the gap could allow for sustaining a plasma discharge leading to the entire M1 being in an erosion dominated regime explaining a lack of any edge deposits contrary to that observed at $\alpha = 45^{\circ}$. This is however a speculation, and further studies are necessary to verify this.

The results have several implications for mirror cleaning in ITER diagnostic systems. They indicate that FM cleaning in presence of a $\lambda/4$ filter is promising in strong magnetic fields given that the wall deposition on M1 can be strongly reduced, contrary to strong wall depositions observed when similar experiments were performed in absence of any magnetic field [16]. The net deposition on M1 as well as M2, however, is significantly dependent on the geometry of the FMU, $A_{\mathrm{g}}/A_{\mathrm{p}}$ as well as the orientation of the FMU in the magnetic field. Our results imply that the minimum distance between the M1 and the adjacent walls should be sufficiently large (>15 mm) to prevent any edge deposition on the M1. Furthermore, since the plasma column follows the direction of magnetic field, one can predict the exact portions of the FMU walls in ITER which would be in contact with plasma, and accordingly engineer the FMU geometry in order reduce their sputtering and/or deposition on M1 as well as M2.

It is worth noting that while we use Cu as the wall material in our FMU mock-up, the walls in most of the diagnostic ducts and FMUs in ITER are expected to be made of stainless steel [35]. However, in terms of physical properties, i.e. sputtering energy threshold and erosion yield with He projectile, steel is in the range of Cu. Hence the results obtained with Cu walls give a very good estimate of the impact of wall sputtering and deposition that can be expected in ITER diagnostic systems [16].

4. Conclusion and outlook

In this study, we experimentally investigated the influence of a 3 T magnetic field on the RF discharges, wall sputtering and deposition on FMs in an ITER sized mock-up of a first mirror unit with Cu walls. The FMU consisted of two electrodes M1 and M2 serving as the first and second mirrors, wherein M1 was powered and M2 grounded. Studies were done in both the DC-decoupled scheme (without $\lambda/4$ filter), where M1 develops a negative self-bias voltage, and the DC-coupled scheme (with $\lambda/4$ filter) where the M1 is DC-grounded. In the former, the influence of process parameters, particularly the RF power and the FM orientation in the magnetic field, on the self-bias voltage developed on M1 was investigated. In the latter, long exposure RF discharge experiments were done in different orientations of the FMU with respect to the magnetic field to study the wall sputtering and deposition on FMs during the experimental discharge.

The presence of a strong magnetic field significantly influenced the generated plasma, confining the discharge in a beam originating from M1 and extending in the direction of the magnetic field. Consequently, the plasma column wets only a portion of the FMU wall. In the DC-decoupled scheme (without $\lambda/4$ filter), this considerably influences the self-bias voltage that develops on M1. At the same RF power and pressure, changing the orientation of FMU in the magnetic field can change the self-bias voltage on M1 by as much as a factor of 100, which is a direct consequence of the changing wetted area by the plasma beam. The self-bias voltage also increases with RF power due to an increase in the ionization

potential. However, for any given parameter the self-bias voltage is maximum in the absence of a magnetic field owing to the fact that the discharge wets the entire FMU compared to a limited portion in the presence of a magnetic field.

The variation in the wetted area by the plasma column also has a notable influence on the wall sputtering and deposition in the DC-coupled scheme (with $\lambda/4$ filter), where M1 is DC-grounded. At $\alpha = 45°$ where $A_g/A_p \sim 1$, the plasma beam sputters the wet wall surface on the FMU, which leads to an edge deposition on M1. However, most of the M1 surface was free of wall deposits, while M2 recorded a minuscule wall deposition at the rate of $\sim$1 nm h^{-1}. At $\alpha = 20°$ the plasma beam sputters a larger wall surface adjacent to M1 and M2 since $A_g/A_p \sim 2.7$. In this configuration, the entire surface of M1 was free of wall deposits while M2 recorded a much larger deposition with an average rate of $\sim$13 nm h^{-1}.

The results provide considerable insight into the RF plasma cleaning of FMs in ITER in the presence of strong magnetic fields. In particular, the discharge is confined in a beam with the bounds of the FM, eventually wetting a region of the FMU in the diagnostic system in the direction of the toroidal magnetic field. In ITER, there are diagnostics systems that will implement FM cleaning in either DC-decoupled or DC-coupled schemes. For the FM cleaning in the DC-decoupled scheme, the ion energy at the mirror depends considerably on the self-bias voltage on the FM and is equivalent to $e(V_p - V_{DC})$. Our results indicate, that the V_{DC} and hence the ion energy on the FM depends not only on the ionizing potential but also on the orientation of the FM with the magnetic field. While V_{DC} depends on the FM orientation, so does the wet FMU wall area A_g which is eventually sputtered. Hence, the FM orientation with magnetic field in ITER could utilise an optimum position in order to lower the A_g, increase the distance between the wet area and the mirrors, as well achieve the desired V_{DC} on the FM. For the FM cleaning in the DC-coupled scheme, FMU wall deposition was considered a major issue in absence of a magnetic field [16]. However, our results indicate that in strong magnetic fields the DC-grounded M1 is primarily in an erosion dominated regime, and the wall deposition is limited primarily to the edge. Furthermore, the wall deposition on M1 can be completely eliminated at lower angles α where the connection length between M1 and the wet wall surface is increased. However, at lower α the overall A_g increases and so does the deposition on M2. This can however be reduced as well by using mitigation strategies like floating wall components at the wet surface of the FMU [16], or grids between the mirrors and the FMU wall [17].

The results call for further work in the area of FM cleaning in strong magnetic fields. The properties of plasma and in particular the measurement of V_p is a major issue in magnetic fields. Research is necessary on this topic, in order to determine the absolute ion energies at the walls and electrodes in strong magnetic fields. Experiments are also necessary to verify the role of floating wall components and grounded grids in lowering the wall sputtering by the plasma beam. While we have established that wall deposition is not a major problem in FM cleaning with $\lambda/4$ filter, the same cannot be said of the erosion homogeneity of the FMs. Further work is required to study the erosion profile and homogeneity of the FMs in strong magnetic fields. This is currently under investigation by the authors of this work, whose results will be discussed in a future publication.

Acknowledgments

This work was supported by the ITER Organization under I/O Contract IO/18/CT/4300001749. This work has also been carried out within the framework of the EUROfusion Consortium and has received funding from the Euratom research and training programme 2014–2018 and 2019–2020 under Grant Agreement No. 633053. The views and opinions expressed herein do not necessarily reflect those of the ITER Organization or European Commission. Swiss Federal Office of Energy, Swiss Nanoscience Institute, Swiss National Science Foundation and the Federal Office for Education and Science are acknowledged for their financial support.

ORCID iDs

Kunal Soni https://orcid.org/0000-0002-8786-7365
Roland Steiner https://orcid.org/0000-0002-4350-4132
Rodrigo Antunes https://orcid.org/0000-0001-9993-7247
Lucas Moser https://orcid.org/0000-0003-1766-9942
Laurent Marot https://orcid.org/0000-0002-1529-9362
Ernst Meyer https://orcid.org/0000-0001-6385-3412

References

[1] Mukhin E.E. *et al* 2011 *Nucl. Fusion* **52** 013017
[2] Walsh M. *et al* 2015 Integration of diagnostics on ITER *2015 IEEE 26th Symp. Fusion Engineering (SOFE)* (Piscataway, NJ: IEEE) pp 1–8
[3] Moon S., Petersson P., Rubel M., Fortuna-Zalesna E., Widdowson A., Jachmich S., Litnovsky A., Alves E. and Contributors J. 2019 *Nucl. Mater. Energy* **19** 59–66
[4] Ivanova D. *et al* 2014 *Phys. Scr.* **T159** 014011
[5] Shigin P. *et al* 2021 *Fusion Eng. Des.* **164** 112162
[6] Chabert P. and Braithwaite N. 2011 *Physics of Radio-Frequency Plasmas* (Cambridge: Cambridge University Press)
[7] Soni K., Moser L., Steiner R., Mathys D., Le Guern F., Piqueras J., Marot L. and Meyer E. 2019 *Nucl. Mater. Energy* **21** 100702
[8] Soni K., Moser L., Porosnicu C., Antunes R., Arredondo R., Dinca P., Steiner R., Marot L. and Meyer E. 2022 *J. Nucl. Mater.* **564** 153671
[9] Dmitriev A.M. *et al* 2017 *Phys. Scr.* **T170** 014072
[10] Ushakov A. *et al* 2018 *Fusion Eng. Des.* **136** 431–7
[11] Campbell D.J. *et al* 2019 *J Fusion Energ* **38** 11–71
[12] Soni K. *et al* 2021 *Plasma Phys. Control. Fusion* **63** 045005
[13] Köhler K., Coburn J.W., Horne D.E., Kay E. and Keller J.H. 1985 *J. Appl. Phys.* **57** 59–66
[14] Aanesland A., Charles C., Boswell R.W. and Lieberman M.A. 2005 *Phys. Plasmas* **12** 103505
[15] Faudot E., Ledig J., Moritz J., Heuraux S., Lemoine N. and Devaux S. 2019 *Phys. Plasmas* **26** 083503
[16] Soni K., Steiner R., Antunes R., Moser L., Shigin P., Reichle R., Marot L. and Meyer E. 2021 *Nucl. Fusion* **61** 126017
[17] Soni K., Antunes R., Steiner R., Moser L., Marot L. and Meyer E. 2022 *Plasma Sources Sci. Technol.* **31** 075009
[18] Leipold F. *et al* 2016 *Rev. Sci. Instrum.* **87** 11D439

[19] Shaw D. and Wagenaars E. 2019 *Plasma Phys. Control. Fusion* **61** 085031
[20] Razdobarin A.G. *et al* 2015 *Nucl. Fusion* **55** 093022
[21] Rogov A.V., Kapustin Y.V. and Alekseev A.G. 2015 *Instrum. Exp. Tech.* **58** 161–6
[22] Marot L., Linsmeier C., Eren B., Moser L., Steiner R. and Meyer E. 2013 *Fusion Eng. Design* **88** 1718–21
[23] Moser L., Steiner R., Leipold F., Reichle R., Marot L. and Meyer E. 2015 *J. Nucl. Mater.* **463** 940–3
[24] Moser L. *et al* 2017 *Phys. Scr.* **T170** 014047
[25] Yan R. *et al* 2017 *Nucl. Fusion* **58** 026008
[26] Marot L. *et al* 2021 *Fusion Eng. Des.* **163** 112140
[27] Pouchou J. and Pichoir F. 1993 *Scanning Microsc.* **7** 12 (https://digitalcommons.usu.edu/microscopy/vol1993/iss7/12)
[28] Rickerby D.G. and Thiot J.-F.O. 1994 *Mikrochim. Acta* **114–115** 421–9
[29] Galbert F. 2007 *Microsc. Microanal.* **13** 96–7
[30] Moser L. 2017 Plasma cleaning of diagnostic first mirrors for the nuclear fusion machine ITER *PhD Thesis* University of Basel
[31] Chodura R. 1982 *J. Nucl. Mater.* **111–112** 420–3
[32] DeWald A.B., Bailey A.W. and Brooks J.N. 1987 *Phys. Fluids* **30** 267–9
[33] Yamamura Y. and Shindo S. 1984 *Radiat. Effects* **80** 57–72
[34] Guterl J., Bykov I., Ding R. and Snyder P. 2021 *Nucl. Mater. Energy* **27** 100948
[35] Pitts R.A. *et al* 2015 *J. Nucl. Mater.* **463** 748–52